RSC Advances

ROYAL SOCIETY OF CHEMISTRY

www.rsc.org/advances

Research Article RA-ART-09-2014-009709 R-2

Catalytic Pretreatment of Biochar residues derived from Lignocellulosic Feedstock for Equilibrium Studies of Manganese, Mn (II) cations from aqueous solution

Zaira Zaman Chowdhury,[1, 2]* Md. Rakibul Hasan[1] , Sharifah Bee Abd Hamid[1], Emy Marlina, Sharifuddin Mohd. Zain[2], and Khalisanni Khalid [2,3]

[1] Nanotechnology and Catalysis Center (NANOCAT), University Malaya, Kuala Lumpur 50603, Malaysia, zaira_chowdhury@live.com, zaira.chowdhury76@gmail.com, rakibhhc130022@siswa.um.edu.my, dr.sbeehamid@gmail.com, marlinasamsuddin76@gmail.com

[2] Departments of Chemistry, Faculty of Science, University Malaya, Kuala Lumpur 50603, Malaysia, smzain@um.edu.my

[3] Malaysian Agricultural and Research Institute (MARDI), Selangor 43400, Malaysia, sanni@mardi.gov.my

† These authors contributed equally to this work.

* Author to whom correspondence should be addressed; E-Mail: zaira.chowdhury76@gmail.com
Tel.: +60102675621 (ext. 123); Fax: +60- 97694205.

Received: 27/06/2014/ Accepted: / Published:

Abstract: This research aims to pretreat and activate the biochar sample for sorption studies of Mn(II) cations from synthetic wastewater. The Bio-char initially synthesized by physical activation of dried *Hibiscus canabilis L* stems. The synthesized char were pretreated with a strong metal hydroxide catalyst of potassium hydroxide (KOH). The secondary phase of activation was conducted by using carbon dioxide gas. Batch adsorption was conducted to delineate the effect of agitation time; temperature and initial cation concentration in synthetic solution. Adsorption kinetics was studied by analyzing the experimental data using Pseudo First, Pseudo Second, Elovich and Intra Particle Diffusion Models. Mathematical simulation after linearization of aforementioned kinetic models showed that the adsorption kinetics was mainly governed by Elovich and Pseudo second order kinetics. This indicated that Mn(II) cations were mainly chemically adsorbed by means of complex formation with the active functional groups present on the surface of the pretreated and activated biochar. Langmuir, Freundlich and Temkin isotherm models were used at different temperature to elucidate the sorption performance of the equilibrium system. Langmuir maximum monolayer adsorption capacity obtained was 31.25 mg/g at 30 $^{\circ}$C. Thermodynamic parameters were evaluated. Negative values of Gibb's free energy, ΔG° ensures feasibility of the equilibrium system. The process was endothermic as the enthalpy change, ΔH° obtained for the process was positive.

Keywords: equilibrium system; kinetics; isotherm; thermodynamics, adsorption

1. Introduction

Lignocellulosic biomass is regarded as one of the most advantageous precursors to obtain carbon rich materials. However, depolymerizing the intricate lignocellulosic network of biomass to produce biochar with sufficient porosities is challenging. Biomass substrates are ubiquitous and cheap. Moreover, biomass residues contain low ash and high volatile materials. Thus, conversion of lignocellulosic biomass to solid char (carbon) with specific properties is economically sustainable. The distinctive structures of the biomass in rapports with porosities as well as surface functional groups can produce efficient adsorbent materials. This will resolve the waste disposal problem with accumulation of value added products. Nevertheless, the application of untreated biomass residues has some limitations. Their surface area per unit mass is comparatively less without treatment. Furthermore the situation becomes worst due to leaching of some organic chemicals from untreated biomass into the process stream.[1] Up to date, different types of physicochemical techniques using liquid acid, base or metallic salt catalysts have been implemented to activate biochar substrate for further application. Lot of efforts has been made by previous researchers to prepare carbonaceous adsorbent from waste biomass to remove inorganic and organic pollutants from waste water. [2, 3, 4, 5, 6]

Presence of inorganic metallic cations in aqueous stream is hazardous as it affects overall ecosystem adversely.[7, 8, 9] The metallic cations accumulate into the food chain because they are non-biodegradable.[10, 11, 12] Different types of heavy metals such as, arsenic (As), mercury (Hg), lead (Pb), nickel (Ni), copper (Cu), zinc (Zn), manganese (Mn), iron (Fe) etc. are present in waste water. Careless discharge of industrial effluents as well as some anthropogenic activities has enriched the aqueous stream with these heavy metals.[13, 14] Specially due to mining activities, process effluents enriched with Mn (II) ions are entering into the water bodies. Divalent cations of manganese, Mn^{2+} and it's metalloids are frequently found in iron (Fe) containing waste sludge. If it is inhaled at a concentration greater than > 10 mg/day, it can cause brain damage and neurological disorder in human. It can cause permanent stains on fabric also.[15] Removal of Mn(II) cations by adsorption technique is somewhat difficult because it is the last member of Irving William series. Thus it is fairly reluctant to form stable complexes with the functional groups onto the adsorbent surface and thereby eliminated by sorption mechanism from wastewater. Mn^{2+} ions can be removed by oxidizing it and subsequently precipitate it as MnO_2. This process exhibits slower kinetics below pH 8. In that case secondary pollutant of rhodochrosite $(MnCO_3)_4$ is produced.[15] Recently activation of bio-char derived from lignocellulosic biomass has gained importance by the researchers' up to a greater extent. Pyrolysis of lignocellulosic substrate can produce solid, liquid or gaseous products like char, light oils, viscous tars and gases. However, the proportion of different products obtained throughout pyrolysis processes is considerably prejudiced by the type of catalysts or the methodology used for chemical pretreatment.[16, 17] Certain alkali, acid or metallic salt can act as catalyst to promote the formation of carbonaceous adsorbent materials having enlarged surface area with sufficient porosities. Presence of this type of catalyst in certain amounts during the pyrolysis process can enhance char yield through dehydration reactions and degradation of tars.[17]

The objective of this study is to pretreat the bio-char synthesized from dried stems of *Hibiscus canabilis L. Hibiscus cannabinus L*, is a plant of *Malvaceae* family which has similar characteristics like jute. It is an annual or biennial herbaceous plant growing up to 1.5-3.5 m tall containing a woody base. The stems are usually 1–2 cm diameter, often but not always branched. The fibres are found in the bast (bark) and core (wood) of stems or stalks of the plant. After alkaline pretreatment, the char was activated at high temperature and used for removal of Mn (II) cations from synthetic waste water. Batch adsorption was carried out to analyze the effect of initial metal ion concentration, contact time, pH and temperature. The subsequent section describes the physiochemical characteristics of the prepared char samples. Equilibrium kinetics, isotherm and thermodynamics studies were conducted to determine the process parameters influencing the sorption process.

2. Experimental

2.1. Preparation of adsorbent Bio char

The woody stem were collected and cut into 1-2 mm. The samples were washed vigorously to remove dirt and dried at 110 °C for 24 hours. At first carbonization of 50 g of dried stalks was carried out in a tubular furnace by flowing N_2 gas at 400 °C temperature for 2 hours. The carbonized biochar was pretreated with KOH where the impregnation ration between char and KOH was kept at 1:7 with addition of 500 ml water to dissolve the alkali pellets completely. The mixture was heated at 90-100 °C for 6 hours to ensure effective penetration of the base to remove unburnt tarry constituents from the surface of the char. Resultant char with KOH solvent was dried in oven at 105 °C to dry the sample entirely. Pretreatment with base catalyst will aid in unclogging the pores which will subsequently increase the surface area. The final step of pyrolysis was conducted by pyrolysis in presence of carbon di oxide gas at temperature (585±1) °C for 1 hr 45 minutes.

Yield is the ratio of final activated adsorbent with the original biomass residues before pyrolysis. Yield was calculated by using equation 1:

$$Yield = \frac{W_2}{W_1} x100 \qquad (1)$$

Here,

W_2= Dry weight after activation (g)

W_1= Dry weight of the original biomass residues before pyrolysis (g)

The samples were washed for several times with hot de-ionized water to remove residual alkali. Few drops of hydrochloric acid (0.1 molar) were used during washing the sample and it was washed until the pH of the washing solutions reached around 6.5-7. The samples were dried and crushed to fine powders. The activated adsorbent thus obtained was sieved through sieve No 200µm. The yield obtained was 38.77%. Finally it was stored in desiccator over fresh silica gel for sorption studies.

2.2. Preparation of Adsorbate solution

The stock solution of Mn (II) ions having concentration range of 1000 mg/l was prepared by using requisite amount (2.95 g) of $MnCl_2.2H_2O$ salt in 1000 ml distilled water. The batch adsorption experiments were conducted by diluting the stock solution to prepare test solution having concentration ranges from 50 mg/l, 60 mg/l, 70 mg/l, 80mg/l, 90 mg/l and to 100 mg/l.

2.3. Surface characterization of un activated and activated Bio char

The BET surface area along with micro pore, meso pore volume and diameter were determined by Autosorb-1, Quantachrome Autosorb surface analyzer. Elemental composition that is percentage of carbon, hydrogen, nitrogen and others were measured by using Ultimate Analyzer (PerkinElmer-Series II 2400, USA). Iodine number and bulk density of the prepared sample was determined by following the process depicted earlier in the literature. [18] Fixed carbon content of the sample along with remaining ash residues, volatile matter and moisture content of both the sample was determined by TGA Analyzer (Model Perkin Elmer TGA7, US). Surface functional groups were identified by FTIR analysis (Model Perkin Elmer FTIR-2000, US). Raw biomass, unactivated and activated biochar

were dried and crushed with KBr. The sample mixed with KBr was pressed to form transparent pellets. Spectra were measured in the range between 4000 and 400 cm^{-1}.

2.4. Batch adsorption studies

A series of conical flasks were loaded with 0.2 g of activated char and 50 ml of Mn (II) cations solution having desired concentration range in a water bath equipped with cover to maintain the fixed temperature. The solutions were agitated at 150 rpm for different temperature. The pH of the solution was adjusted to 5.5 before sorption studies by using 0.1 M HCl acid. The water samples were withdrawn at different time interval and analyzed to measure remaining metal ion concentration. The amount adsorbed onto the surface of the biochar and removal percentages were calculated by equations 2 and 3 respectively: [19]

$$q_e = \frac{(C_0 - C_e)V}{W} \quad (2)$$

$$\%\,\mathrm{Re}\,moval = \frac{C_0 - C_e}{C_0} x100 \quad (3)$$

Here, q_e (mg/g) shows the solid phase concentration that is amount of ion adsorbed onto the surface of char at equilibrium. C_o is the initial metal ion concentration, C_e (mg/L) is the liquid-phase concentrations of Mn(II) ions at equilibrium conditions. V (L) is the volume of the synthetic solution, and W (g) is the mass of activated biochar taken. [18, 19] Each experiment was triplicated under identical condition and average results were used for calculation. The experiment was repeated at 30 ◦C, 50 ◦C and 70 ◦C for thermodynamics studies. The conical flasks containing activated char (0.2 g) with 50 ml of test solution was sealed and agitated by using water bath shaker equipped with cover to prevent heat loss. Experimental data obtained was used for kinetics, isotherm and thermodynamics study by using Sigma Plot, version 10.

3. Results and Discussion

3.1. Physio-chemical properties of un activated and activated Bio char

Fig. 1(a-c) illustrates the morphology of raw stem of *Hibiscus canabilis L*; unactivated and activated biochar. The raw stem or stalk surface was comparatively smooth with some irregular shape pores (Fig. 1-a). The surface of KOH pretreated carbonized char before activation was coarse with few pores (Fig. 1-b). The pores formed after carbonization stage is constricted and tapered. Some lumps of tarry substances are deposited blocking the pores. During carbonization, volatile materials are diffusing out of the carbon matrix into the gas main stream. Some of the constituents might have a collision with the pore walls, which cause hydro cracking and eventually result in carbon deposition. [20] For preparing guava seed based activated carbon, it was observed that carbonization step unaided by activation did not yield adsorbent materials with enough porosity due to inadequate decomposition of organic constituents present inside the carbonaceous residues. Therefore, the pores were considerably blocked by the remains of carbonization products.[21] Thus after activation in presence of carbon dioxide gas flow, substantial bulks of semicircular pores were developed on the surfaces of the bio chars (Fig. 1-c). This implies that alkali pretreatment with secondary stage of activation has effectively catalyzed the development of new pores which can subsequently increase the sorption rate.

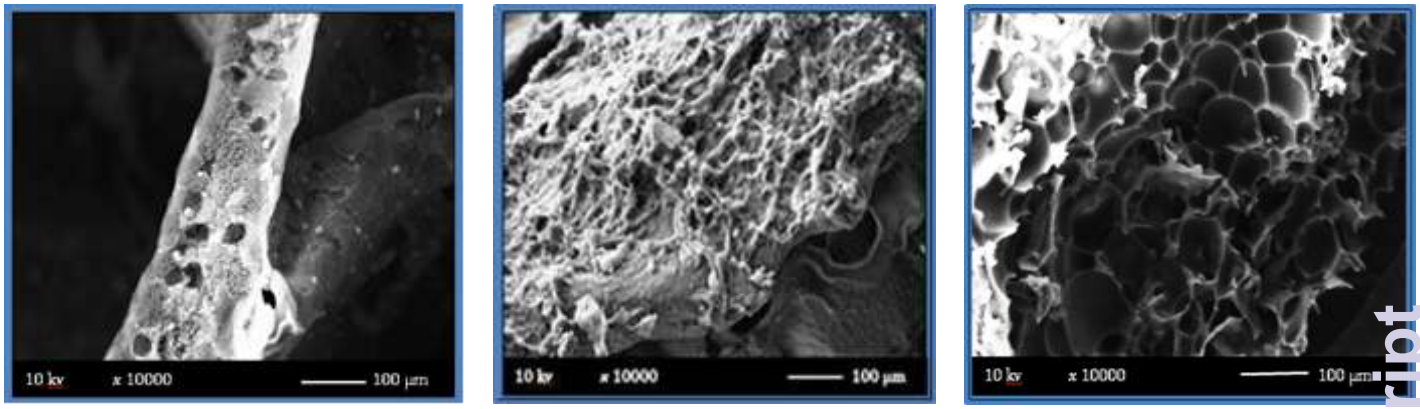

(a) Raw Biomass (b) Unactivated char (c) Catalytically Activated char

Fig. 1 Scanning Electron Micrograph (SEM) of (a) Raw Biomass (b) Unactivated Char (c) Catalytically Activated Char

Chemical interactions between adsorbent and adsorbate molecules are predominated by oxygen containing surface functional groups.[22] The FTIR peaks obtained for raw biomass, unactivated carbonized char sample along with treated and activated char samples are illustrated by Fig. 2.

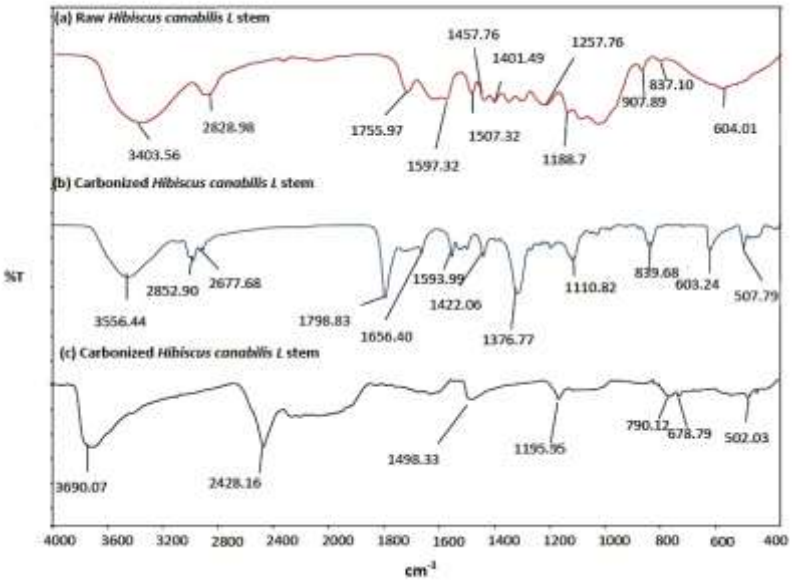

Fig. 2 FTIR spectra of (a) Raw Biomass (*Hibiscus canabilis L* or kenaf stem) (b) Carbonized unactivated stem (c) Pretreated activated stem

There were significant differences between the spectrums of raw biomass, unactivated and activated char sample. In the region of 3403-3690.07 cm^{-1}, the spectrum of all the samples showed broad and strong bands. This showed that hydroxyl groups exist before and after activation. The peaks around 1755.97 and 1798.83 cm^{-1} in raw and unactivated biomass became indiscernible after activation. The trend of the FTIR spectrum for the raw biomass, as well as unactivated and activated biochar samples contains some peaks, which are almost similar. Some peaks around 2800–2900 cm–1, 1500–1610 cm–1 and

1100 cm−1 were representing C–H stretching of alkane, the C=C stretching of the aromatics and the C–O–C stretching vibration of the esters, ether and phenol groups. C=O stretching vibration of carboxyl groups were observed around 1400-1550 cm^{-1}. Some peaks were observed at 500-900 cm^{-1} which was assigned for C-H out-of plane bending and O-H stretching vibrations of C-O-H band. Table 1 summarizes the significant peaks and their assignment for raw biomass, unactivated and catalytically activated biochar sample.

Table 1 List of FTIR peaks observed for Native biomass, untreated and activated Bio Char

IR peak	Frequency (cm^{-1})			Peak Assignment
	Raw Biomass	Unactivated Bio Char	Activated Bio Char	
1	-	-	474.53	C-H out-of-plane bending
2	-	507.79	502.03	C-H out-of-plane bending
3	604.01	603.24	-	C-O-H bending
4	-	-	790.12	C-H out-of-plane bending
5	837.10	839.68	-	C-H out-of-plane bending
6	907.89	-	-	O-H bending
7	1188.70	1110.82	1195.95	-C-O-C stretching
8	1257.76	-	-	C-O-C stretching
9	-	1376.77	-	CH_3 deformation
10	1401.49	1422.06	1498.33	in-plane OH bending and C-O stretch of dimmers
11	1597.32	1593.99	-	C=C ring stretching of benzene derivatives
12	-	1656.40	-	C=O stretching
13	1755.97	1798.83	-	C=O stretching
14	-	-	2428.16	C=C stretching vibration of ketones, aldehydes or carboxylic group
15	-	2677.68	-	C=C stretching vibration of ketones, aldehydes or carboxylic group
16	2828.98	2852.90	-	C-H stretching
17	3403.56	3556.44	3690.07	O-H stretching vibration of hydroxyl functional groups

After base catalytic activation by using KOH, a lot of peaks changed their frequency level or, in certain cases, disappeared. An analogous phenomenon was observed by previous researchers during preparing carbon from raw pistachio nut shell[23]. The research findings showed that different oxygen groups, which were initially present in the raw pistachio nut shell, disappeared after the heat treatment. This was due to aromatization of the carbonaceous materials. After base impregnation and activation of rice straw, the peak intensities of the ester groups and phenolic ether groups were decreased significantly. The researchers concluded that pyrolysis in the presence of KOH might destroyed the lignin content comprising the ester and ether linkages after the activation of rice straw[24].

The N_2 adsorption isotherm is shown by Figure 3. The curve represent Type I isotherm with three distinct regions: the first part is comparatively steeper; obtained for nitrogen uptake at $P/P_0 < 0.2$, the second part is almost parallel to X-axis which is observed for P/P_0 values between 0.2-0.8 and the third part shows small upward bend at $P/P_0 \approx 0.9$. The characteristics of the isotherm shows presence of high proportion of micropores with small amount of meso and macropores.[18]

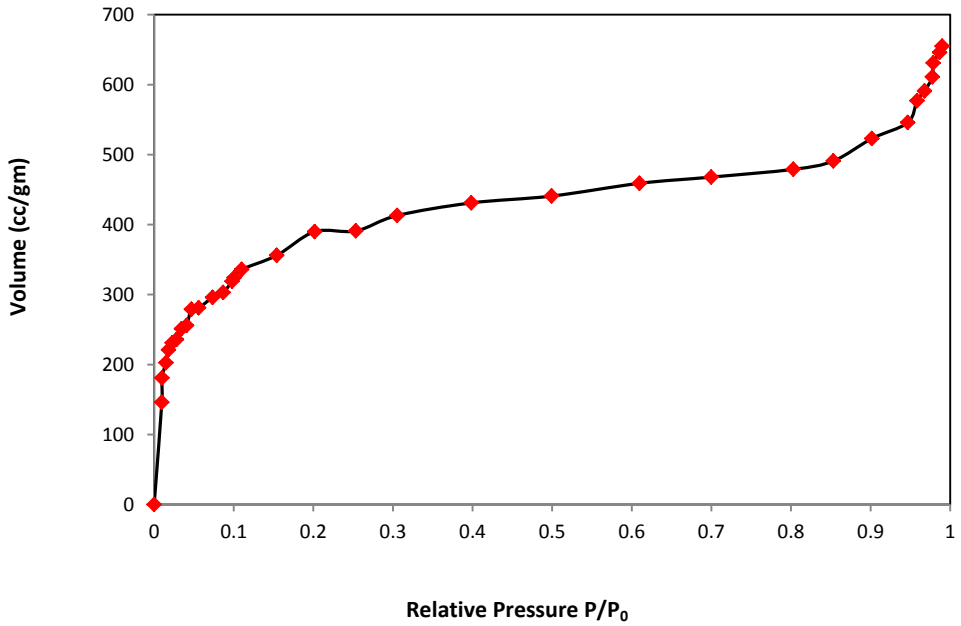

Fig. 3 N_2 Adsorption Isotherm

The BET surface area along with micropore volume has been summarized in Table 2. The surface area of the carbonized char increased drastically after base pretreatment and activation process. Micropore surface area of the unactivated char was increased from 1.30 m^2/g to 1004.30 m^2/g after activation process. Total pore volume of biochar increased almost six times from 0.1025 cc/g to 0.6065 cc/g after activation process (Table 2). The average pore diameter of the activated char was 23.02 Å representing mesoporous texture of the prepared char. [25] Stavropouios and Zabaniotou (2005) described the reaction mechanism of KOH with lignocellulosic char sample[8]. Their findings revealed that, at first stage of activation, KOH would dehydrate to produce K_2O. K_2O would react further with CO_2 by the water-shift reaction to yield K_2CO_3 during the second phase of activation. Thus, intercalation of metaltic potassium is reported for the drastic expansion of the surface area of the activated char sample. This type of activation would finally provide enlarged specifie surface area with high pore volume[26, 27] .

Table 2 Physico-chemical Characteristics of Unactivated and Activated Biochar

Sample Properties	Unactivated Char	Activated Biochar
BET surface area	2.02 m^2/g	1062.04 m^2/g
Micropore Surface area	1.30 m^2/g	1004.30 m^2/g
Total pore volume	0.1025 cc/g	0.6065 cc/g
Average pore diameter	3.02 Å	23.02 Å
BJH cumulative adsorption surface area	1.22 m^2/g	657.82 m^2/g
Bulk Density	0.498 g/mL	0.349 g/mL
Iodine Number	4.03 mg/g	789.09 mg/g

The fixed carbon and ash content was more in the activated bio char rather than the raw and unactivated samples. Volatile matter was decreased after the activation process. At high temperature, the organic compounds were released as gas and liquid products from lignocellulosic matrix.[19] Ultimate analysis (Table 3) showed that, the carbon content of the sample increased from 57.05% to 70.09% after activation of the biochar. This illustrated that two step base catalytic activation method using CO_2 gas was appropriate enough to produce adsorbent materials competent for removal of Mn^{2+} cations from aqueous solution. It was observed that, elemental carbon content was slightly higher than fixed carbon determined by proximate analysis. Hydrogen content was reduced after the activation process. Nitrogen content decreased after activation process.

Table 3 Proximate and Ultimate Analysis of Unactivated and Activated Biochar

Proximate Analysis	Unactivated Char	Activated Bio Char
Moisture	5.05	3.09
Volatile Matter	57.19	19.51
Fixed Carbon	32.54	69.96
Ash	5.22	7.04
Ultimate Analysis	**Unactivated Char**	**Activated Biochar**
Percentage Carbon	57.05	70.09
Percentage Hydrogen	13.49	7.51
Percentage Nitrogen	5.04	1.31
Others	24.42	21.37

3.2. Effect of initial pH

In order to investigate the effect of initial pH on adsorption uptake, the solution pH was changed from 2-12 while keeping the other variables of agitation speed, contact time, temperature and activated biochar amount constant. Following Fig. 4 describes the effect of pH on removal percentage of Mn(II) cations onto activated biochar.

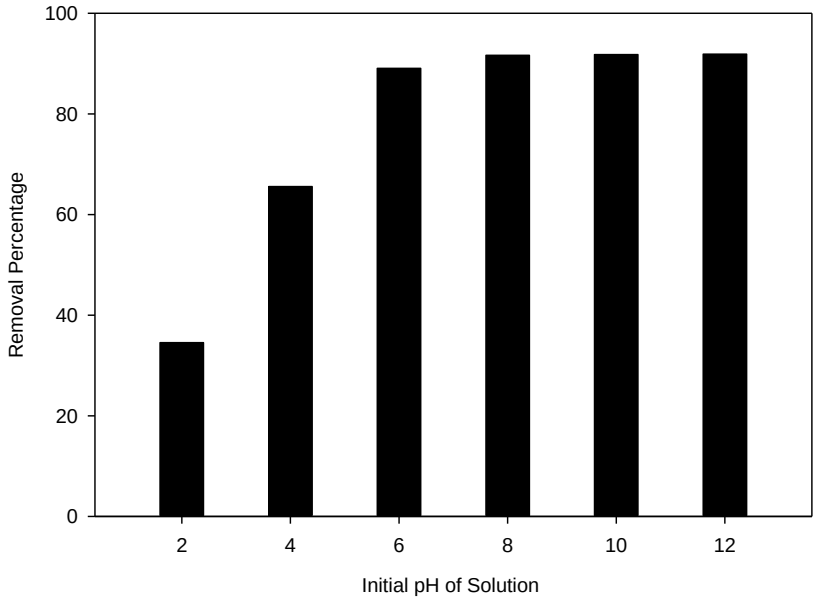

Fig. 4 Effect of pH on removal percentage of Mn(II) cations from water (Initial concentration: 100 mg/L, Temperature: 30 ˚C, Agitation Speed: 150 rpm, Contact Time: 180 minutes, Activated Biochar: 0.2g)

Adsorption of cation is strongly dependent on the surface functional groups and pH value of the solution. At lower pH of 2, the adsorption was very low. It rapidly increased between pH 4 to 6. After that for increasing pH up to 12, there was slightly increase in removal percentage. In acidic pH about 2–3, H^+ and H_3O^+ ions are present inside the solution. This competes with positive cations during sorption with subsequent lower removal efficiency.[28, 29] Basically at pH 5.5-6, divalent cations of Mn^{2+} can exist either as metallic Mn^{2+} cations or in its hydroxide form in aqueous solution. The –OH and –COOH functional groups present on the surface of the activated char sample can initiate following reactions to enable the overall elimination process from aqueous solution.

1. $(–SO^+H_2) + Mn^{2+} \rightarrow (SO)\ Mn + 2H^+$
2. $(–SO^+H_2) + Mn\ (OH)^+ \rightarrow (–SO)\ MnOH + 2H^+$
3. $nS–COOH + Mn^{2+} \rightarrow (S–COO)_n\ Mn + nH^+$

Here, S represents the surface of the activated bio-char sample. Carboxylate group (–COOH) identified on the surface of the activated sample can dissociate around pH 5. –COOH groups have pKa values 3-5. Mn^{2+} can react to form surface complexes according to reaction 3. A Similar reaction phenomenon was reported for the adsorptive removal of Cu^{2+} cations by orange peel, saw dust and bagasse sample.[30] At basic pH from 8-12, cumulative effect of adsorption and precipitation might occur.[31] That is why, to evade collective outcome of adsorption and precipitation, equilibrium studies were conducted at pH 5.5.

3.3. Effect of adsorbate concentration and contact time

Agitation time influences the formation of the external film which creates a boundary layer over the surface of the sorbent. The extent of dispersion of the solute within equilibrium contact time in case of batch sorption process is a crucial factor as it affects the process of overall mass transfer. Thus the

residual equilibrium concentration, C_e (mg/l) with respective sorption amount, q_t (mg/g) was measured at predetermined interval of time. As can be seen from all these plots, the first sharper region is completed within the initial 40 minutes time reflecting immediate sorption or external surface sorption. This represents the mass transfer of the sorbate cations from the bulk solution to the sorbent surface. The second region, almost parallel to X-axis is the gradual sorption stage. The involvement of different stages in the entire sorption process indicates that the adsorption rate is initially faster and then it becomes slower near to the equilibrium time. For initial 40 minutes of contact, the curves obtained for all the concentration range was steeper reflecting high affinity of the adsorbent materials towards the adsorbate cations. Thus for initial stage of adsorption process, adsorption uptake q_t (mg/g) increased with time. This stage was rapid due to availability of active sites capable of capturing the metallic cations under investigation. After that, the uptake was almost constant yielding straight lines almost parallel to x-axis. After 150 minutes, the uptake was negligible. The system reached equilibrium within 180 minutes.

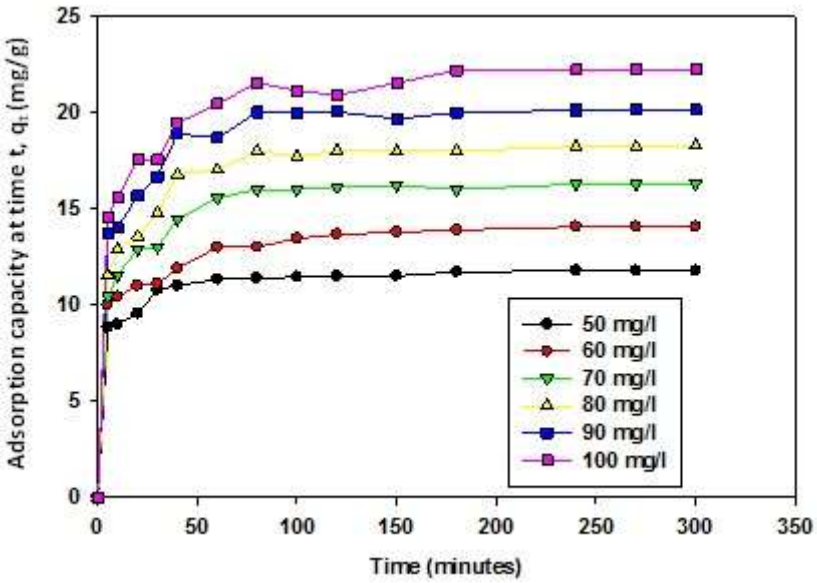

Fig. 5 Effect of contact time with concentration and equilibrium uptake at pH 5.5, agitation speed 150 rpm and temperature 30 ˚C

3.4. Equilibrium kinetics studies

Estimation of kinetic parameters will deliver noteworthy information regarding the overall sorption process. The suitability of explicit types of kinetic models can be confirmed by both the correlation coefficient, R^2 and the normalized standard deviation percentages, Δq (%) in numerous literatures. The equation can be written as:

$$\Delta q\ (\%) = 100\sqrt{\frac{\Sigma[(q_{t,exp}-q_{t\,cal})/q_{t,exp}]^2}{(N-1)}} \qquad (4)$$

Where, N means the number of data points, $q_{t,exp}$ and $q_{t,cal}$, (mg/g) are the experimental and calculated adsorption uptake at time t, respectively.[18, 32, 33]

Following equations (5) and (6) are used to determine the rate constants by using pseudo-first-order kinetic model:[34, 35]

$$\log(q_e - q_t) = \log q_e - \frac{K}{2.303}\, t \qquad (5)$$

$$h = K_1 q_{e,cal} \qquad (6)$$

Here, K_1 (l/min.) represents the rate constant, h (mg/g-min) is the initial rate of sorption, q_e and q_t are the amount of cation (mg/g) adsorbed at equilibrium contact time and at any time t (minute) respectively. The linear plots of log (q_e-q_t) versus t (mins.) are shown by Fig. 6.

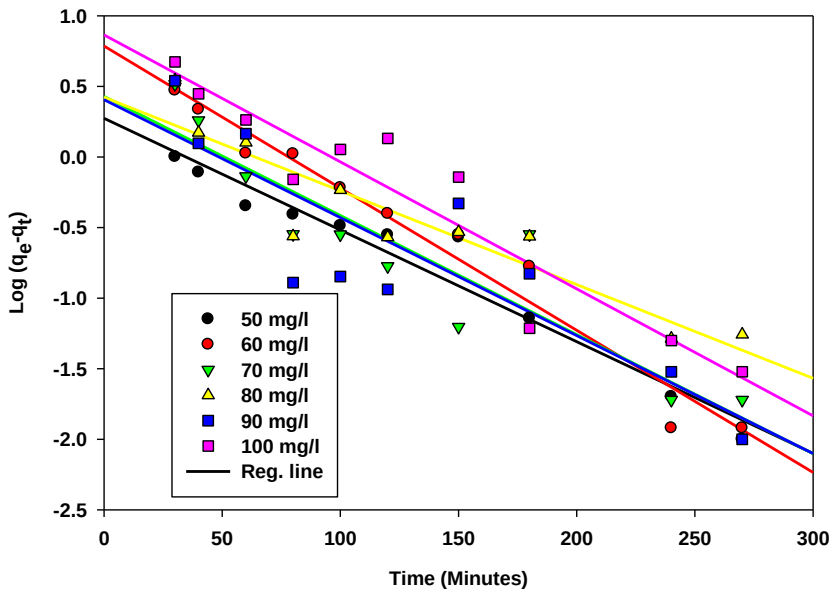

Fig. 6 Linear Plots of Pseudo First Order Kinetics of Manganese, Mn (II) cations sorption at pH 5.5, agitation speed 150 rpm and temperature 30 ˚C

Pseudo-second-order kinetics is expressed by using following linear equations (7) and (8): [20, 21, 36, 37]

$$\frac{t}{q_t} = \frac{1}{K_2 q_e^{\,2}} + \frac{1}{q_e} t \qquad (7)$$

$$h = K_2 q_{e_{cal}}^2 \qquad (8)$$

Where, the rate constant of second-order adsorption is K_2 (g/mg-min), uptake at any time is q_t (mg/g), uptake at equilibrium is q_e (mg/g) and h (mg/g-min) is the initial rate of sorption. The linear plots of t/q_t, versus t (mins.) give $1/q_e$ as the slope and $1/k_2q_e$ as the intercept and are shown by following Fig. 7. The physical parameters related to First and Second order Kinetics were determined and listed in Table 3.

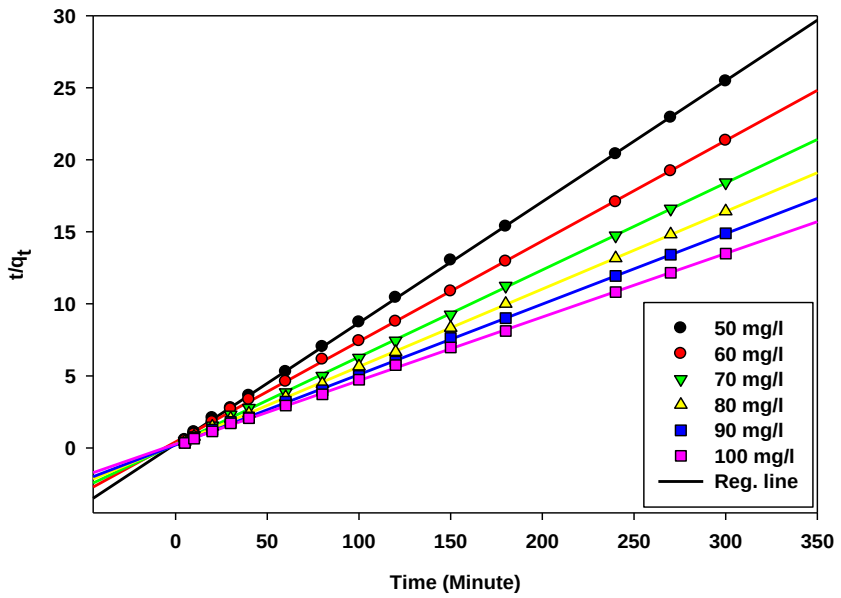

Fig. 7 Linear Plots of Pseudo Second Order Kinetics of Manganese, Mn (II) cations sorption at pH 5.5, agitation speed 150 rpm and temperature 30 ˚C

Table 4 Pseudo-First and Pseudo-Second Order Model constants for different initial concentration at pH 5.5, agitation speed 150 rpm and temperature 30 ˚C

				Pseudo First Order Kinetics					Pseudo Second Order Kinetics				
Initial Concentration, C_0 (mg/L)	Equilibrium Concentration, C_e (mg/L)	$q_{e,(exp)}$ (mg/g)	% Removal	$q_{e,(cal)}$ (mg/g)	K_1 (g/mg-min)	h (mg/g-min)	R^2	Δq%	$q_{e,(cal)}$ (mg/g)	K_2 (g/mg-min)	h (mg/g-min)	R^2	Δq%
50	2.876	11.781	94.248	2.506	0.0184	0.046	0.960	22.7	11.905	0.0242	3.430	0.999	0.28
60	3.756	14.061	93.740	5.296	0.0210	0.111	0.974	17.9	14.493	0.0113	2.374	0.999	0.35
70	4.852	16.287	93.068	3.917	0.0200	0.078	0.898	21.9	16.667	0.0130	3.611	0.999	0.55
80	6.908	18.273	91.365	4.276	0.0161	0.068	0.893	22.1	18.868	0.0105	3.738	0.999	0.55
90	8.500	20.375	90.560	4.325	0.0138	0.059	0.844	22.7	20.834	0.0112	4.861	0.999	0.63
100	11.00	22.250	89.000	7.638	0.0201	0.154	0.930	18.9	22.727	0.0072	3.719	0.999	0.60

Equilibrium data were fitted with Elovich model to explicate the chemisorption nature of the adsorbate-adsorbent system under investigation by using following linear equation: [18]

$$q_t = \frac{1}{b} Ln(ab) + \frac{1}{b} Lnt \qquad (9)$$

Where, a (mg/g-h) represents initial sorption rate; b (g/mg) is the activation energy for sorption. The linear plots of Elovich model is illustrated by following Fig. 8.

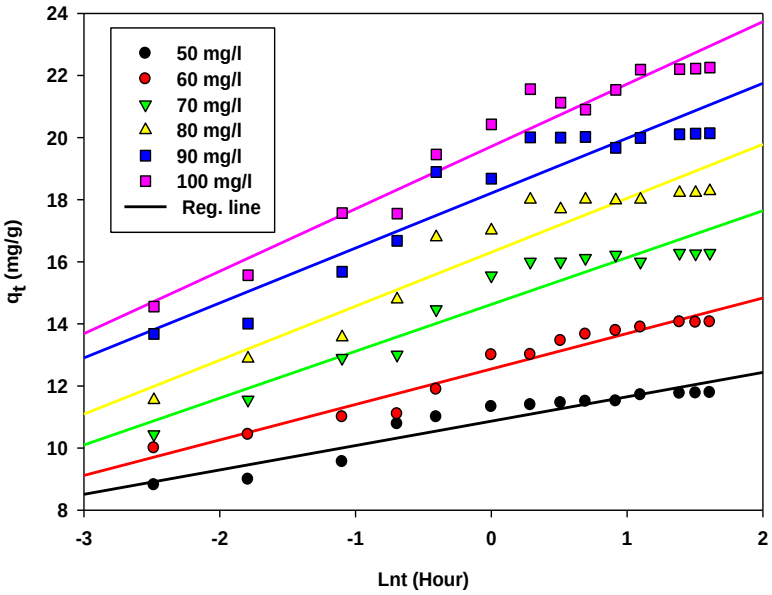

Fig. 8 Linear Plots of Elovich Model of Manganese, Mn (II) cations sorption at pH 5.5, agitation speed 150 rpm and temperature 30 ˚C

Elovich model rate constants were determined from the linear plots (Fig. 8) and summarized in Table 4. It is observed that the values of 1/b ln (ab) and 1/b increase with the increase of initial concentration range studied. This trend is expected because as the concentration range increases, a relatively large number of adsorbate ions will strike with the active sites of the adsorbents to form surface complexes. Eventually more uptakes by the prepared adsorbents will be observed.[19]

Table 5 Elovich Model Rate Constant for Different Initial Concentration at pH 5.5, agitation speed 150 rpm and temperature 30 ˚C

Initial Concentration (mg/L), C_0	ln (ab)1/b	1/b	R^2	$q_{e,cal}$ (mg/g)	Δq%
50	10.86	0.785	0.898	12.123	0.81
60	12.54	1.142	0.954	14.377	0.62
70	14.62	1.509	0.913	17.048	1.30
80	16.30	1.738	0.907	19.097	1.25
90	18.21	1.769	0.887	21.057	0.93
100	19.71	2.009	0.949	22.943	0.86

It is observed that the R^2 values (Table 4) obtained for the Pseudo second order kinetics are better than those obtained earlier from the Pseudo-first-order and Elovich equation. The Δq% values obtained for Pseudo second order model were smaller than Pseudo first order model. This confirms that the cations were adsorbed chemically onto the surface of the activated char.

3.5. Intra-particle Diffusion Mechanism

Intra-particle diffusion model was fitted with the experimental data to analyze diffusion process at solid-liquid interface. It is represented by following equation:[38]

$$q_t = K_{dif} t^{0.5} + C \qquad (10)$$

The intra-particle diffusion rate constant, K_{dif} (mg/g h) and diffusion constant C are obtained from slope and intercepts of the linear plots of q_t (mg/g) versus $t^{0.5}$ (hour) shown by Fig. 9.

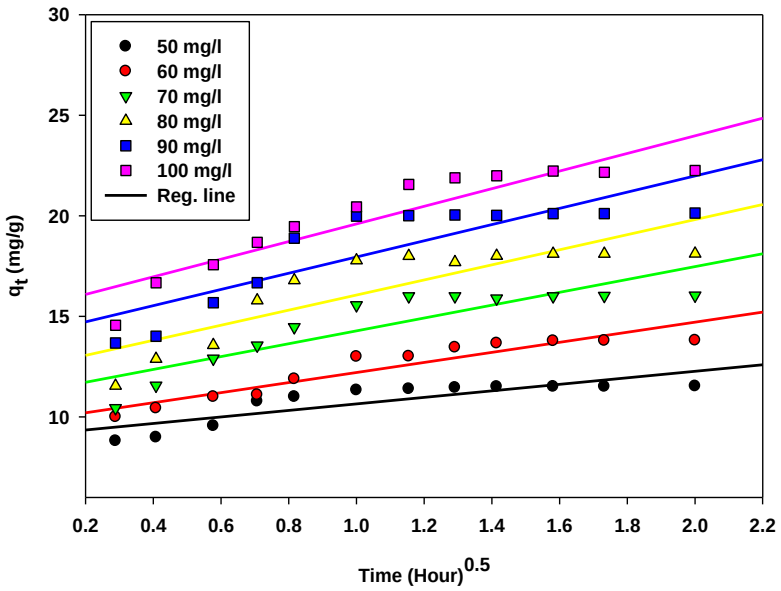

Fig. 9 Linear Plots of Intra-particle Diffusion of Manganese, Mn (II) cations sorption at pH 5.5, agitation speed 150 rpm and temperature 30 °C

The R^2 values obtained here were less than the other models used here. The lines contained intercepts and did not cross the origin. This suggested that along with the pore diffusion, several other mechanisms have influence in the rate controlling stage.[18, 19] Similar phenomenon has been reported in our previous work for sorption studies of Pb (II) cations by using *Mangostana Garcinia* based activated carbon.[19] Table 6 summarizes the model parameters.

Table 6 Intra- Particule Diffusion Model Rate Constant for Different Initial Concentration at pH 5.5, agitation speed 150 rpm and temperature 30 °C

Initial Concentration (mg/L), C_0	C	K_{dif} ($mg/gh^{0.5}$)	R^2	$q_{e,\,cal}$ (mg/g)	Δq%
50	9.307	1.418	0.671	12.483	1.65
60	10.13	2.185	0.799	15.016	1.88
70	11.66	2.614	0.666	17.505	2.07
80	12.87	3.121	0.669	19.849	2.39
90	14.73	3.161	0.648	21.798	1.94
100	15.61	3.728	0.747	23.946	2.11

It is found that the values of the constant C for all the samples generally increase with increasing initial concentrations of the solution. This trend is expected due to the greater driving force of sorbate cations (increase in effective numbers of collisions between cations and active sites) at higher concentration.[39]

3.6. Equilibrium Isotherm Analysis

Langmuir, Freundlich, and Temkin were used to fit equilibrium data obtained at three different temperatures of 30 °C, 50 °C and 70 °C. The nonlinear form of Langmuir equation can be expressed as:[38]

$$q_e = \frac{K_L C_e}{1 + a_L C_e} \tag{11}$$

The linear form of Equation 8 can be shown by:

$$\frac{C_e}{q_e} = \frac{1}{q_{\max} K_L} + \frac{1}{q_{\max}} C_e \tag{12}$$

Here, q_{max} (mg/g) represent maximum monolayer adsorption capacity. K_L is Langmuir adsorption constant (l/mg) related to binding energy for sorption. R_L is the separation factor obtained from Langmuir equation:

$$R_L = \frac{1}{1 + K_L C_o} \tag{13}$$

For this study, R_L values are determined for all the initial concentration under investigation (50 mg/l-100 mg/l). Based on the magnitudes of the separation factor R_L, specific knowledge about the categories of the isotherm can be anticipated (Table 7).

Table 7 Types of Isotherm based on Separation Factor R_L

Value of R_L	Types of Isotherm
$R_L > 1$	Unfavorable
$R_L = 1$	Linear
$0 < R_L < 1$	Favorable
$R_L = 0$	Irreversible

The multilayer sorption performance of the prepared char sample can be analyzed by using Freundlich isotherm. This also indicates the surface heterogeneity of the sample. The nonlinear equation is established on the proposition that the active sites over the adsorbent surface are disseminated exponentially with the heat of sorption process. [41] It is shown by:

$$q_e = K_f C_e^{1/n} \tag{14}$$

The linear form of Freundlich isotherm is expressed by:

$$\ln q_e = \ln K_f + \frac{1}{n} \ln C_e \tag{15}$$

Here, K_f (mg/g)(l/mg)$^{1/n}$ is the affinity factor of the adsorbate towards the adsorbent and 1/n represents intensity of adsorption respectively.[41]

Table 8 Isotherm Model parameters at 30°C, 50°C and 70°C Temperature

Temp.	**Initial concentration**		**Langmuir**			**Freundlich**			**Temkin**		
°C	(mg/l)	R_L	q_{max} (mg/g)	K_L (l/mg)	R^2	K_F (mg/g) (l/mg)$^{1/n}$	1/n	R^2	B	K_T (l/mg)	R^2
30	50	0.084	31.25	0.217	0.992	7.698	0.445	0.980	7.328	1.788	0.989
	60	0.071									
	70	0.062									
	80	0.054									
	90	0.049									
	100	0.043									
50	50	0.070	32.26	0.263	0.951	8.819	0.426	0.974	0.919	7.088	0.937
	60	0.059									
	70	0.052									
	80	0.045									
	90	0.041									
	100	0.037									
70	50	0.063	37.03	0.296	0.942	9.708	0.503	0.973	2.504	8.596	0.950
	60	0.053									
	70	0.046									
	80	0.041									
	90	0.036									
	100	0.033									

Temkin isotherm postulates that the heat of sorption required for all the adsorbate molecules in the layer would reduce linearly with the degree of surface acquaintance due to adsorbent-adsorbate

interactions. Equilibrium data has been further fitted with Temkin isotherm. The nonlinear equation used to depict Temkin Isotherm is expressed by: [42]

$$q_e = \frac{RT}{b} \ln K_T C_e \qquad (16)$$

The linear form of Equation 13 can be expressed as:

$$q_e = \frac{RT}{b} \ln K_T + \frac{RT}{b} \ln C_e \qquad (17)$$

Here, RT/b = B (j/mol), denotes Temkin constant which depicts the heat of sorption process whereas K_T (L/g) reflects the equilibrium binding constant. R (8.314 J/mol k) is universal gas constant and T° (K) is absolute solution temperature.[42] From Table 8, it can be observed that Langmuir separation factor, R_L and Freundlich exponent 1/n are below one which represents favorable adsorption processes.[43] The linear regression obtained for different isotherm models are illustrated by Fig. 10.

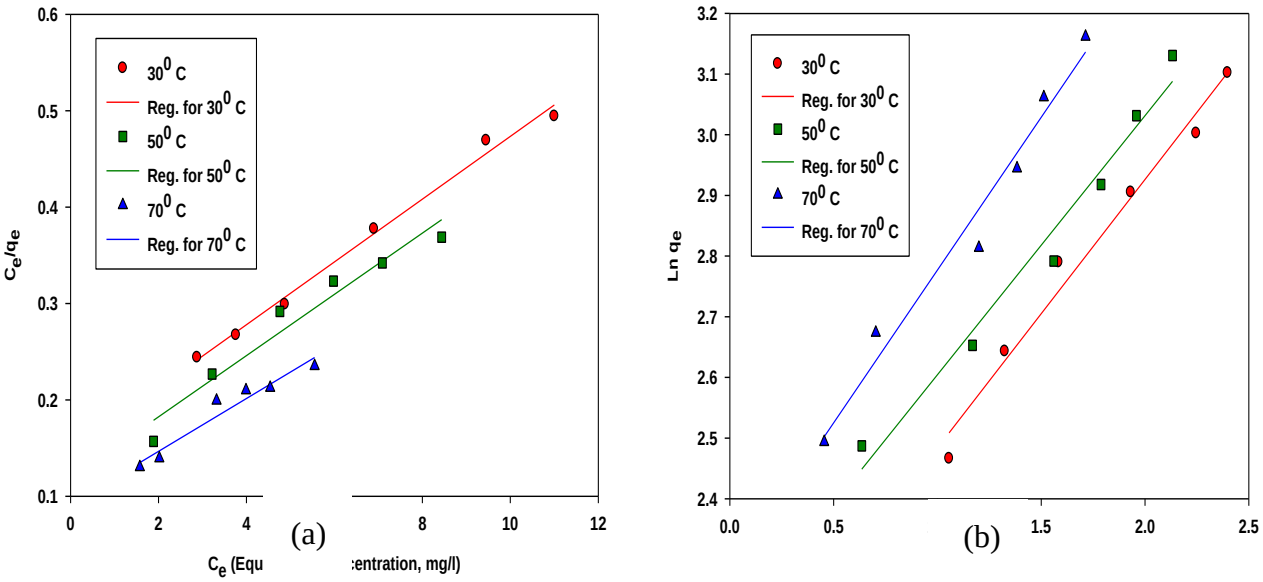

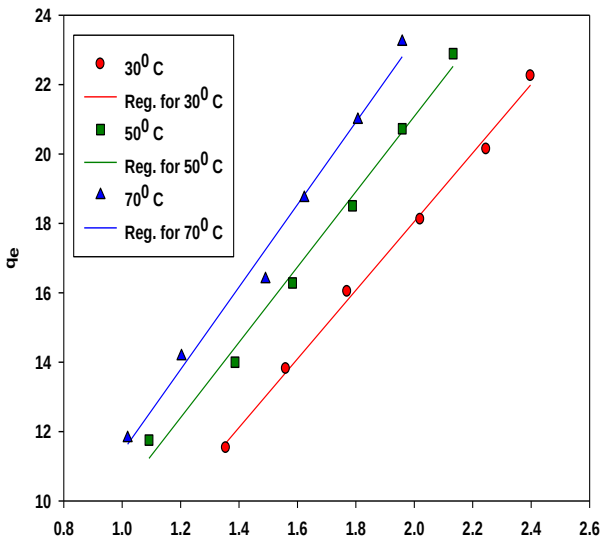

(c)

Fig. 10 Linear Regression Analysis of (a) Langmuir, (b) Freundlich and (c) Temkin Isotherm model at different temperature.

3.7. Thermodynamics characterization

Thermodynamic studies were conducted to evaluate the magnitudes of Gibbs free energy (ΔG°), enthalpy (ΔH°), and entropy (ΔS°) of the sorption process.[44] The linear equation used in this context is listed below:

$$Ln\ K_L = \frac{\Delta S}{\Delta R} - \frac{\Delta H}{RT} \quad (18)$$

$$\Delta G = RT\ Ln\ K_L \quad (19)$$

Here, constant K_L (l/mg) was obtained from Langmuir equation at three different temperatures. R is a physical constant regarded as universal gas constant (8.314 j/ mol. K). It has been used in many thermochemical equations and relationship. T is the absolute temperature in Kelvin scale. The linear plot of ln K_L versus 1/T was used to calculate thermodynamic parameters and listed in Table 8. The positive magnitude of the enthalpy (ΔH°) obtained here reflects endothermic sorption process. [43, 44] This trend was consistent with Langmuir maximum monolayer capacity, q_m and Freundlich affinity factor, K_F evaluated earlier in Table 8. The increase of temperature from 30 $^{\circ}$C to 70 $^{\circ}$C has increased the values which imply that the uptake capacity of Mn (II) cations is favored by elevation of temperature. In case of endothermic reactions, increase in temperature would increase the rate of diffusion of the adsorbate species across the external boundary layer as well as inside the pores of the adsorbent particle. This might be due to the decrease in the viscosity of the solution.[45] It was depicted also that the active surface sites increased proportionally with the increase in temperature. [46] The entropy, ΔS° determined was positive showing increased degree of freedom. This also showed increased randomness at solid-solution interface. Gibbs free energy change, ΔG° was negative. That

means the adsorption process is feasible and spontaneous for the temperature range under investigation. [44] Similar observation has been reported in our studies for sorption of Mn(II) cations onto activated palm ash. [31]

Table 8 Thermodynamic parameters of Mn (II) sorption onto activated char

Temperature, °K	ΔG° (Kj-mol^{-1})	ΔH° (Kj-mol^{-1})	ΔS° (jK^{-1} mol^{-1})	R^2
303	-3.8441	+6.7041	+0.0095	0.9901
323	-3.5852			
343	-3.4710			

4. Conclusions

Base catalytic approach to activate biochar sample derived from waste biomass residues of kenaf stalk was successful. Activated char sample had enlarged surface area than the unactivated one. It was efficient enough to remove 94.248% of Mn^{2+} cation from 50 mg/l solution at 30 ◦C. Kinetic studies were conducted in terms of Pseudo first order, Pseudo second order and Elovich model. Reaction mechanisms are studied by using Intra particle diffusion models. However, the best correlation values with small standard deviation percentages were obtained for Elovich and Pseudo second order kinetic models. Isotherm data were generated by using the linear form of Langmuir, Freundlich and Temkin isotherm model. Adsorption isotherm was well fitted by Freundlich isotherm confirming surface heterogeneity. Increasing temperature had progressive influence on removal efficiency inferring endothermic nature of sorption. It can be concluded that activated biochar based carbon is compatible enough for adsorption of Mn^{2+} ions from single solute system up to a greater extent. The future perspective of this research is to observe the applicability of activated biochar sample for a multi-solute system containing different other competitive metallic cations.

Acknowledgments

The authors are grateful for the financial support from High Impact Research (HIR F- 000032) and Bright Spark Scholarship for their cordial support to complete this work.

References

1. Z. Z. Chowdhury, S. B. Abd Hamid, R. Das, M. R. Hasan, S. M. Zain, K. Khalid and M. N. Uddin, *Bioresources* 2013**, 8(4)**, 6523.
2. Z. K. George, *Materials*, 2012, ***5***, 1826.
3. A. A. Ahmad and B. H. Hameed, *J. Hazard. Mater.*, 2010**, 173**, 487.
4. A. A. Ahmad, B. H. Hameed and A. L. Ahmad, *J. Hazard. Mater.* 2009, **170,** 612.
5. M. C. Baquero, L. J. Giraldo, C. Moreno, F. Suarez-Garcia, A. Martinez-Alonso, J. M.D. Tascon, *J. Anal. Appl. Pyrol.*, 2003, **70**, 779.
6. J. N. Sahu, J. Acharya and B. C. Meikap, *Bioresource Technol.*, 2010, **101**, 1974.
7. J. Dai, F. Ren and C.Y. Tao, *Molecules*, 2012, **17**, 4388.

8. G. G. Stavropoulos and A.A. Zabaniotou, *Micropor. Mesopor. Mat.*, 2005, **83**, 79.

9. Y. Bulut and Tez Zeki. *J. Enviro. Sci.*, 2007, **19**, 160.

10. A. Aklil, M. Moutflih and S. Sebti, *J. Hazard. Mater*. 2004, **A112**, 183.

11. P. Srivastava and S.H. Hasan, *Bioresources*, 2011**, 6(4),** 3656.

12. L. Tofan, C. Paduraru, V. Irina and O. Toma, *Bioresources*, 2011**, 6(4),** 3727.

13. J. M. Lezcano, F. González, A. Ballester, M.L. Blázquez, J. A. Muñoz, C. García-Balboa, *J. Environ. Manage.*, 2011, **92**, 2666.

14. J. M. Lezcano, F. González, A. Ballester, M.L. Blázquez, J. A. Muñoz, C. García-Balboa, *Chem. Ecol*, 2010, **26(1),** 1.

15. C. M. Juan, G. Rigoberto and G. Liliana, *Materials*, 2010**, 3**, 452.

16. W.T. Tsai, C.Y. Chang and S.L. Lee, *Bioresource Technol*., 1997, **64**, 211.

17. K. Gergova and S. Eser, *Carbon*, 1996, **34**, 879.

18. Z. Z. Chowdhury, Preparation, Characterization and Adsorption studies of heavy metals onto Activated Adsorbent Materials derived from agricultural residues. PhD Thesis, University Malaya, Malaysia, 2013**.**

19. Z. Z. Chowdhury, S.M. Zain, A. K. Rashid, K. Khalisanni and R. F. Rafique, *Bioresources*, 2012, **7 (3),** 2895.

20. M. Kamishita, O.P. Mahajan and P.L. Walker, *Fuel*, 1977, **56**, 444.

21. I.A. Rahman and B. Saad, *M. J. Chem.*, 2003, **5**, 8.

22. I. S. Johari, N. A. Yusof, Md. J. Haron and S. M. Mohd Nor, *Molecules*, 2013, **18**, 8461.

23. T. Yang and A. C. Lua, *J. Colloid Interf. Sci.*, 2003, **267,** 408.

24. G. H. Oh, C. H. Yun and C. R. Park, *Carbon Sci*, 2003, **4**, 180.

25. Z. Hu, M. P. Srinivasan and N. Yaming, *Carbon*, 2001, **39**, 877.

26. R.L. Tseng, and S.K. Tseng, *J. Colloid Interf. Sci.*, 2005, **287**, 428.

27. J.M. Salman, and B. H. Hameed, *J. Hazard. Mater.*, 2010, **175**, 133.

28. Z. Z. Chowdhury, S.M. Zain and A. K. Rashid, *E J. Chem.* 2011, **8(1),** 333.

29. Y. Wu, J. Cao, P. Yilihan, Y. Jin, Y. Wen and J. Zhou, *RSC Adv.*, 2013, 3, 10745.

30. A. Habib, N. Islam, A. Islam and A.M.S. Alam, *Pak. J. Anal. Environ. Chem.*, 2007, **8,** 21.

31. Z.Z. Chowdhury, S.M. Zain, A.K. Rashid and K. Khalid, *Orient. J. Chem.* 2011, **27**, 405.

32. A. S. Bhatt, P. L. Sakaria, M. Vasudevan, R. R. Pawar, N. Sudheesh, .H. C. Bajaj and H. M. Mody, *RSC Adv.*, 2012, 2, 8663.

33. B. H. Hameed, A.A. Ahmad, and N. Aziz, *Chem. Eng. J.*, 2007**, 133(1-3),** 195.

34. G. Z. Kyzas and E. A. Deliyanni, *Molecules*, 2012, **17,** 4388.

35. S. Ismadji and S. K. Bhatia, *Carbon*, 2001, **39(8)**, 1237.

36. N. R. Khalili, M. Campbell, G. Sandy and J. Golas, *Carbon* 2000, **38**, 1905.

37. Y.S. Ho and G. McKay, *Chem. Eng. J.* 1998, **70**, 115.

38. M, H. Kalavathy, T. Karthikeyan, S. Rajgopal and L. R. Miranda, *J. Colloid Interf. Sci.*, 2005, **292**, 354.

39. A. Ozer and G. Dursun, *J. Hazard. Mater.*, 2007, **146**, 262.

40. I. Langmuir, *J. Am. Chem. Soc.*, 1918, **40 (9),** 1361.

41. H. M. F. Freundlich, *J. Phys. Chem.*, 1906, **57**, 385.

42. M. J. Temkin and V. Pyzhev, *Acta Physicochemistry*, URSS, 1940, **12**, 217.

43. S. T. Ambrósio, J. C. Vilar Júnior, C. A. Alves da Silva, K. Okada, A. E. Nascimento, R. L. Longo and G. M. A. Campos-Takaki, *Molecules*, 2012, **17**, 452.

44. Z. A. Al Othman, M. Hashem and A. Habila, *Molecules*, 2011, **16**, 10443.

45. S. Chakraborty, S. De, S. Das Gupta and J. K. Basu, *Chemosphere*, 2005**, 58 (8)**, 1079.

46. D. H. K. Reddy, Y. Harinath, K. Seshaiah and A.V.R. Reddy, *Chem. Eng. J.*, 2010, **162 (2),** 626.

Novelty of the work: RA-ART-09-2014-009709

In this research, activated biochar has been produced by base catalytic approach for removal of Mn(II) cations from waste water.